Geophys. J. Int. (2006) **164,** 63–74 doi: 10.1111/j.1365-246X.2005.02810.x

Wavelet-based multiscale resolution analysis of real and simulated time-series of earthquakes

Bogdan Enescu,[1,2] Kiyoshi Ito[1] and Zbigniew R. Struzik[3]

[1]*Disaster Prevention Research Institute (DPRI), Kyoto University, Kyoto, Japan.*
E-mail: benescu@eqh.dpri.kyoto-u.ac.jp
[2]*National Institute for Earth Physics, Bucharest, Romania*
[3]*Graduate School of Education, Tokyo University, Tokyo, Japan*

Accepted 2005 September 10. Received 2005 July 7; in original form 2004 February 27

SUMMARY

This study introduces a new approach (based on the *Continuous Wavelet Transform Modulus Maxima* method) to describe qualitatively and quantitatively the complex temporal patterns of seismicity, their multifractal and clustering properties in particular. Firstly, we analyse the temporal characteristics of intermediate-depth seismic activity ($M \geq 2.6$ events) in the Vrancea region, Romania, from 1974 to 2002. The second case studied is the shallow, crustal seismicity ($M \geq 1.5$ events), which occurred from 1976 to 1995 in a relatively large region surrounding the epicentre of the 1995 Kobe earthquake ($Mw = 6.9$). In both cases we have declustered the earthquake catalogue and selected only the events with $M \geq Mc$ (where Mc is the magnitude of completeness) before analysis. The results obtained in the case of the Vrancea region show that for a relatively large range of scales, the process is nearly monofractal and random (does not display correlations). For the second case, two scaling regions can be readily noticed. At small scales (i.e. hours to days) the series display multifractal behaviour, while at larger scales (days to several years) we observe monofractal scaling. The Hölder exponent for the monofractal region is around 0.8, which would indicate the presence of long-range dependence (LRD). This result might be the consequence of the complex oscillatory or power-law trends of the analysed time-series. In order to clarify the interpretation of the above results, we consider two 'artificial' earthquake sequences. Firstly, we generate a 'low productivity' earthquake catalogue, by using the epidemic-type aftershock sequence (ETAS) model. The results, as expected, show no significant LRD for this simulated process. We also generate an event sequence by considering a 70 km long and 17.5 km deep fault, which is divided into square cells with dimensions of 550 m and is embedded in a 3-D elastic half-space. The simulated catalogue of this study is identical to the case (A), described by Eneva & Ben-Zion. The series display clear quasi-periodic behaviour, as revealed by simple statistical tests. The result of the wavelet-based multifractal analysis shows several distinct scaling domains. We speculate that each scaling range corresponds to a different periodic trend of the time-series.

Key words: earthquake predictability, long-range dependence, (multi)fractals, real and synthetic earthquake sequences, wavelet analysis.

1 INTRODUCTION

The notion of scale-invariance is defined loosely as the absence of characteristic scales of a time-series. Its main consequence is that the whole and its parts cannot be statistically distinguished from each other. The absence of such characteristic scales requires new signal processing tools for analysis and modelling. The *exact self-similar*, scale-invariant processes, like for example the fractional Brownian motion, are mathematically well defined and well documented. In actual real world data, however, the scaling holds only within a finite range and will typically be approximate. Therefore, other 'scaling models' are more appropriate to describe their complexity. Long-range dependence (LRD) or long memory is a model for scaling observed within the limit of the largest scales. Research on LRD (or *long-range correlation*) characteristics of 'real' time-series is the subject of active research in fields ranging from genetics to network traffic modelling. Another broad class of signals corresponds to '*fractal processes*', which are usually related to scaling in the limit of small scales. Such time-series are described by a (local) scaling exponent, which is related to the degree of regularity of a signal. If the scaling exponent varies with position (time), we refer to the corresponding process as multifractal. The fractal concept is,

however, usually used in a broader sense and refers to any process that shows some sort of self-similarity.

(Multi)fractal structures have been found in various contexts, as for example in the study of turbulence or of stock market exchange rates. The concepts of 'fractal analysis' have also been applied to describe the spatial and temporal distribution of earthquakes (e.g. Smalley *et al.* 1987; Turcotte 1989; Kagan & Jackson 1991). Geilikman *et al.* (1990), Hirabayashi *et al.* (1992) and Goltz (1997) have all employed a multifractal approach to characterize the earthquake spatial, temporal or energy distribution. Their results suggest that seismicity is an inhomogeneous fractal process. Kagan & Jackson (1991), by analysing statistically several instrumental earthquake catalogues, concluded that besides the short-term clustering, characteristic for aftershock sequences, there is a long-term earthquake clustering in the residual (declustered or aftershocks-removed) catalogues.

Wavelet analysis is a powerful multiscale resolution technique, well suited to understanding deeply the complex features of real world processes: different 'kinds' of (multi)fractality, LRD, non-stationarity, oscillatory behaviour and trends. The purpose of this study is to apply wavelet analysis to reveal the multifractal and LRD characteristics of the occurrence times of earthquakes. More precisely, we apply the Wavelet Transform Modulus Maxima (WTMM) method that has been proposed as a generalization of the multifractal formalism from singular measures to fractal distributions, including functions (Arneodo *et al.* 1991; Muzy *et al.* 1994; Arneodo *et al.* 1995). By using wavelet analysis, we reveal the clear fractal characteristics of the analysed time-series and successfully describe the main features of our earthquake sequences. The study focuses on the interpretation and explanation of the various temporal fractal patterns found in earthquake time-series and thus, we hope, will be a good reference for future related research. In particular, we try for the first time to discriminate between genuine and spurious LRD due to the presence of simple, trivial trends of the earthquake time-series. The methodology and the detailed characterization of the analysed earthquake time-series may show their usefulness to probabilistic earthquake forecasting, where the inherent complexity (Mulargia & Geller 2003) requires new multiscale analysis tools. In this context, please note that any wavelet method is a compromise between establishing the scale (frequency) or the time accurately, according to the Fourier equivalent of the Heisenberg uncertainty principle. To the best of our knowledge, this is the first systematic study of the multifractal and LRD properties of earthquake time-series by using a wavelet approach. Ouillon & Sornette (1996) have developed a wavelet-based approach to perform multifractal analysis, and applied it in a related field: the study of earthquake fault patterns.

In the next section we introduce the WTMM method and explain the relation between multifractality and wavelets. The WTMM approach is compared in Section 3 with a 'traditional' box-counting technique (BCT) commonly used to estimate the multifractal spectrum. The advantages of using the wavelet method are clearly emphasized. The data to be analysed are introduced in Section 4 and consist of four earthquake time-series. Two of them are real earthquake sequences, while the other two are simulations. Firstly, we generate a sequence of events by using the epidemic-type aftershock sequence (ETAS) model (Ogata 1985, 1988). The second 'artificial' time-series is obtained by using a realistic earthquake model: an inhomogeneous cellular fault embedded in a 3-D elastic solid (Ben-Zion & Rice 1993; Ben-Zion 1996). Section 5 discusses the results of the analysis, while in the last section we present the main conclusions.

2 THE CONTINUOUS WAVELET TRANSFORM (CWT) AND WAVELET-BASED MULTIFRACTAL ANALYSIS

The wavelet transform is a convolution product of the data sequence (a function $f(x)$, where x, referred to in this study as 'position', is usually a time or space variable) with the scaled and translated version of the mother wavelet (basis function), $\psi(x)$. The scaling and translation are performed by two parameters; the scale parameter s stretches (or compresses) the mother wavelet to the required resolution, while the translation parameter b shifts the basis function to the desired location (see Fig. 1a):

$$(Wf)(s,b) = \frac{1}{s}\int_{-\infty}^{+\infty} f(x)\psi * \left(\frac{x-b}{s}\right) dx, \tag{1}$$

where s, b are real, $s > 0$ for the continuous version (CWT) and ψ^* is the complex conjugate of ψ. The wavelet transform acts as a microscope: it reveals more and more details while going towards smaller scales, that is, towards smaller s-values. One can associate with a mother wavelet a purely periodic signal of frequency Fc which 'captures' its main oscillations (Fc is the centre frequency of the mother wavelet). Then, it follows that the frequency corresponding to a certain scale s can be expressed as: $Fs = (SP * Fc)/s$, where SP is the sampling period. As in most wavelet-based multifractal studies and for simplicity, we use 'scale' rather than 'frequency' throughout this paper.

The mother wavelet ($\psi(x)$) is generally chosen to be well localized in space (or time) and frequency. Usually, $\psi(x)$ is only required to be of zero mean, but for the particular purpose of multifractal analysis $\psi(x)$ is also required to be orthogonal to some low order polynomials, up to the degree $n-1$ (i.e., to have n vanishing moments):

$$\int_{-\infty}^{+\infty} x^m \psi(x)\, dx = 0, \qquad \forall m, \quad 0 \le m < n. \tag{2}$$

Thus, while filtering out the trends, the wavelet transform reveals the local characteristics of a signal, and more precisely its singularities. (The Hölder exponent can be understood as a global indicator of the local differentiability of a function.) By preserving both scale and location (time, space) information, the CWT is an excellent tool for mapping the changing properties of non-stationary signals. A class of commonly used real-valued analysing wavelets, which satisfies the above condition (2), is given by the successive derivatives of the *Gaussian* function:

$$\psi^{(N)}(x) = \frac{d^N}{dx^N} e^{-x^2/2}, \tag{3}$$

for which $n = N$. In this study, the analysing wavelet is the second derivative of the *Gaussian*. The computation of the CWT was carried out in the frequency domain, by using the *fast Fourier transform*. The time-series were padded with zeros up to the next power of two to reduce the edge distortions introduced by the Fourier transform, which assumes the data are infinite and cyclic (Torrence & Compo 1998).

It can be shown that the wavelet transform can reveal the local characteristics of f at a point x_o. More precisely, we have the following power-law relation:

$$W^{(n)} f(s, x_0) \sim |s|^{h(x_0)} \tag{4}$$

where h is the Hölder exponent (or singularity strength). The symbol '(n)', which appears in the above formula, shows that the

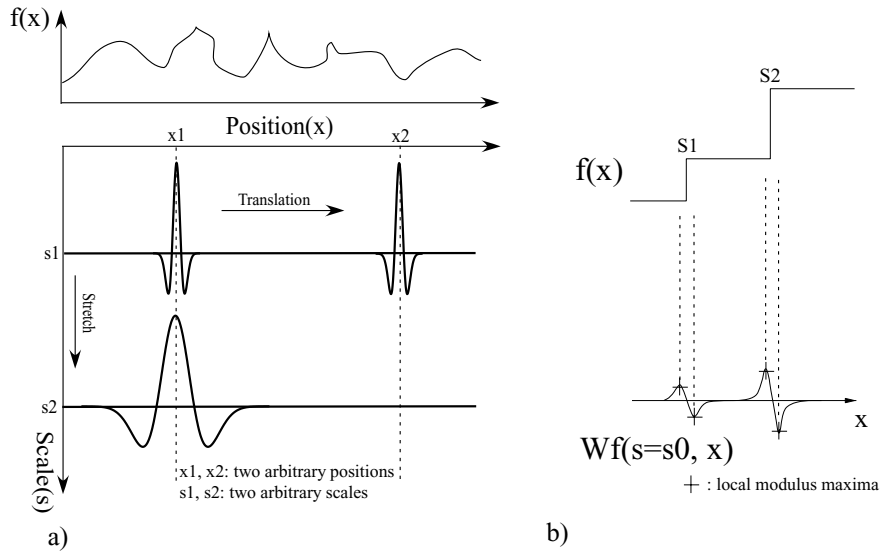

Figure 1. (a) Scaling and translation of the mother wavelet (here the second derivative of the Gaussian) along a signal (function) $f(x)$. The stretching of the wavelet reveals the properties of the signal at progressively larger scales. The wavelet coefficients, computed by using formula (1), are a measure of the similarity between the wavelet and the signal for different positions, x, and scales, s. (b) Up: a function $f(x)$, Down: amplitude of the wavelet transform of function $f(x)$, along the x-axis, at a certain scale, $s0$. The mother-wavelet is the second derivative of the Gaussian. As one goes to finer (smaller) scales (or higher frequencies) the local modulus maxima converge to the singularities of the function (S1 and S2) (adapted from Mallat 1998, Fig. 6.4).

wavelet used ($\psi(x)$) is orthogonal to polynomials up to degree $n-1$. The scaling parameter (the so-called *Hurst exponent*) estimated when analysing time-series by using 'monofractal' techniques is a global measure of self-similarity in a time-series, while the singularity strength h can be considered a local version (i.e. it describes 'local similarities') of the *Hurst exponent*. In the case of monofractal signals, which are characterized by the same singularity strength everywhere ($h(x) = constant$), the Hurst exponent equals h. Depending on the value of h, the input series could be long-range correlated ($h > 0.5$), uncorrelated ($h = 0.5$) or anticorrelated ($h < 0.5$).

The continuous wavelet transform described in eq. (1) is an extremely redundant representation, too costly for most practical applications. To characterize the singular behaviour of functions, it is sufficient to consider the values and position of the WTMM (Mallat & Hwang 1992). The wavelet modulus maximum is a point (s_0, x_0) on the scale-position plane, (s, x), where $|Wf(s_0, x)|$ is locally maximum for x in the neighbourhood of x_0. These maxima are located along curves in the plane (s, x). We present in Fig. 1(b) an example that illustrates the correspondence between maxima lines and the singularities of a function. The WTMM representation has been used for defining the partition function-based multifractal formalism (Muzy *et al.* 1994; Arneodo *et al.* 1995).

Let $\{u_n(s)\}$, where n is an integer, be the position of all local maxima at a fixed scale s. By summing up the q's power of all these WTMM, we obtain the partition function Z:

$$Z(q, s) = \sum_n |Wf(u_n, s)|^q. \tag{5}$$

By varying q in eq. (5), it is possible to characterize selectively the fluctuations of a time-series: positive q's accentuate the 'strong' inhomogeneities of the signal, while negative q's accentuate the 'smoothest' ones. In this work, we have employed a slightly different formula to compute the partition function Z by using the 'supremum method', which prevents divergences from appearing in the calculation of $Z(q, a)$, for $q < 0$ (e.g. Arneodo *et al.* 1995).

Often scaling behaviour is observed for $Z(q, s)$ and the spectrum $\tau(q)$, which describes how Z scales with s, can be defined:

$$Z(q, s) \sim s^{\tau(q)}. \tag{6}$$

If the $\tau(q)$ exponents define a straight line, the analysed signal is a monofractal; otherwise the fractal properties of the signal are inhomogeneous, that is, they change with location, and the time-series is a multifractal. By applying the Legendre transformation to $\tau(q)$ we can obtain the multifractal spectrum $D(h)$. $D(h)$, known also as the singularity spectrum, captures how 'frequently' a value h is found.

When computing the CWT, we introduced some discontinuities at the endpoints of the time-series, due to zero padding. As a result, as one goes to larger scales, the CWT amplitude near the edges decreases as more zeroes enter the analysis. The cone of influence (COI) is defined as the region of the wavelet spectrum, in which such a decrease becomes significant (see Torrence & Compo 1998, for details). When the analysing wavelet is the second derivative of the Gaussian, however, the COI area is relatively small, as the wavelet is relatively narrow. To check for possible border effects, we constructed the WTMM tree by (a) including and (b) excluding the COI region from the analysis. The final results for the two cases were practically the same. This proves that the zero padding did not bias our analysis.

For the computations made in this work, we acknowledge the use of the *Matlab* software package (http://www.mathworks.com), *Matlab*'s *Wavelet Toolbox* and the free software programs: *Wavelab* (Stanford University—http://www-stat.stanford.edu/∼wavelab) (Buckheit and Donoho, 1995), *Fraclab, A Fractal Analysis Software* (INRIA—http://fractales.inria.fr/) and other *Matlab* routines (http://paos.colorado.edu/research/wavelets/; Torrence & Compo 1998). We also developed some routines, in *Matlab*, which are going to be made available on the web (http://www.rcep.dpri.kyoto-u.ac.jp/∼benescu/).

3 ADVANTAGES OF THE WTMM METHOD WHEN COMPARED WITH OTHER TRADITIONAL TECHNIQUES USED TO ESTIMATE THE MULTIFRACTAL DIMENSIONS

To assess the performance of the WTMM approach, we consider a 'classic' example of a recursive fractal function, for which the singularity spectrum can be computed analytically: *the Generalized Devil's Staircase*, associated with the *Multinomial Cantor Measure*. The measure (μ) is constructed by dividing recursively the unit interval [0, 1] in four subintervals of the same lengths and distributing the 'measure' or 'mass' μ among them, with the weights $p1$, $p2$, $p3$ and $p4$ ($p1 + p2 + p3 + p4 = 1$) (Peitgen *et al.* 1992, appendix B). We apply both the WTMM and a 'traditional' box-counting technique (BCT) to characterize the multifractal properties of the multinomial measure and compare their estimates with the theoretical values. Briefly, BCT consists in covering the support (here, the unit interval) with boxes of successively smaller size, ε, and then calculate a partition function for several q-values:

$$Z(\varepsilon) = \sum_{i=1}^{N(\varepsilon)} \mu_i^q, \tag{7}$$

where $N(\varepsilon)$ is the total number of boxes for a certain ε. For each q-value the slope of the linear part of $\log Z(\varepsilon)$ versus $\log(\varepsilon)$ is computed and, thus, the tau-spectrum, $\tau(q)$, can be determined. We refer to Feder (1988) and Peitgen *et al.* (1992) for a detailed description of BCT and other commonly used techniques applied for multifractal analysis.

Fig. 2 presents $\tau(q)$ obtained by using the two methods mentioned above together with the analytical spectrum. One can notice the very good agreement between the theoretical and the computed spectrum, for q-values between -7 and 10, when the wavelet-based procedure is used. The spectrum produced by using the box-counting method, however, shows significant deviations from the theoretical values, especially for negative q. The failure of the standard box counting is mainly the result of a set of boxes with spuriously small mass; when raised to a negative power in the partition function, these boxes become dominating and hence obliterate all information about the original measure (e.g. Grassberger *et al.* 1988). This problem is common for most fixed-size algorithms, including BCT and the method based on the correlation function, which are both used frequently in earthquake-related multifractal studies (Hirabayashi *et al.* 1992). To overcome this problem another sampling procedure, known as the fixed-mass algorithm was adopted (Badii & Broggi 1988) and applied, in the context of earthquakes, by Hirabayashi *et al.* (1992). According to Badii & Broggi (1988), the fixed-radius method works better for $q > 1$, while the fixed-mass method gives better results for $q \leq 1$. However, instead of using two different techniques it is desirable to apply only one reliable method to obtain the whole spectrum, from negative to positive q-values. For larger values of q, the BCT tau-spectrum deviates again slightly from the theoretical one (Fig. 2).

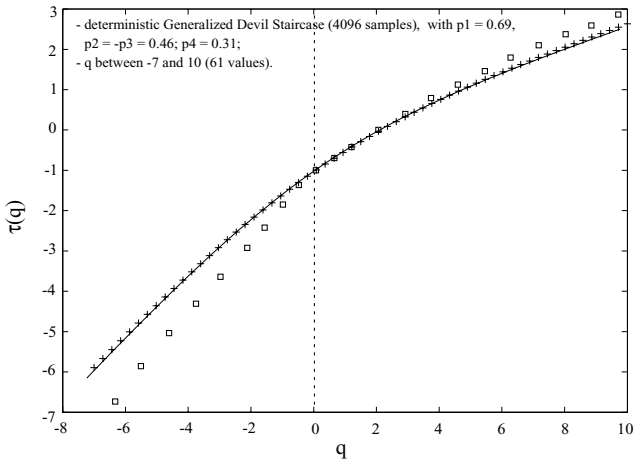

Figure 2. 'Tau-spectrum' for the Generalized Devil Staircase (length of 4096 values). P1, p2, p3 and p4 are the parameters used to obtain the time-series. q takes equally spaced values, between -7 and 10. The spectra computed by using the wavelet approach and the box-counting techniques are represented by crosses and rectangles, respectively. The theoretical spectrum is shown by solid line.

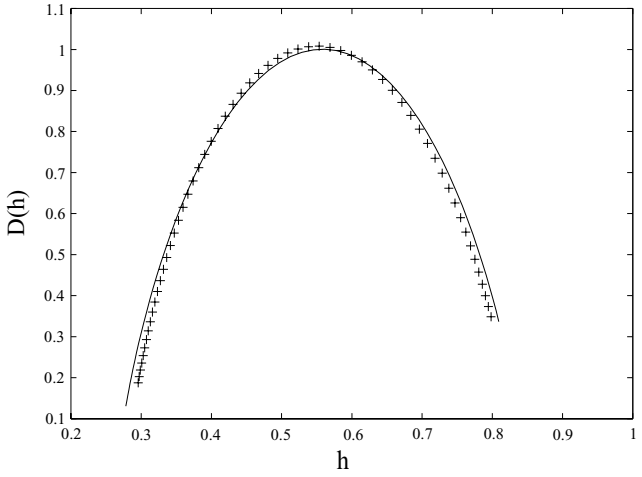

Figure 3. Theoretical (continuous line) and obtained (WTMM method, crosses) $D(h)$ singularity spectrum in the case of the Generalized Devil Staircase. One can notice the clear multifractal signature of the simulated time-series, as well as the good agreement between the theoretical and wavelet-based computed spectrum.

The tau-spectrum in Fig. 2 is curved, which indicates the multifractal nature of the time-series. Fig. 3 presents the theoretical and wavelet-based singularity spectrum, which clearly confirms the non-uniqueness of the Hölder exponent h, and thus the multifractality of the process.

There is another strong argument in favour of the wavelet-based approach: the possibility to discriminate between trivial (polynomial, simple oscillatory) trends and the 'true' fractal behaviour of a time-series (Arneodo *et al.* 1991; Muzy *et al.* 1994; Arneodo *et al.* 1995). In Section 5 we will demonstrate that such trends can mimic LRD and lead to wrong conclusions when a standard technique to quantify the scaling behaviour is used.

4 DATA

We have applied the wavelet-based approach to the analysis of four sets of earthquake data; two of them are real and the other two are simulations. The data consist of interevent times between successive earthquakes above a threshold magnitude. Our choice was made by considering that the earthquake occurrence time is one of the most reliable and accurate parameters that define a seismic event. Also, our choice was based on the relevance of earthquake recurrence times for earthquake hazard and forecasting. The results of the multifractal analysis ($\tau(q)$, $D(h)$) correspond, however, to the integrated interevent times. In this way, we made our results directly

comparable with those obtained by Enescu *et al.* (2005), who use the *Detrended Fluctuation Method* (DFA) to analyse the seismicity of the Vrancea (Romania) region. The method (DFA) requires integrating the data in advance. Nonetheless, the integration just adds a constant value (one) to the obtained h, the results being otherwise identical (Arneodo *et al.* 1995). The four sets of data are explained briefly below.

The Vrancea (Romania) intermediate-depth seismicity

The Vrancea seismic region is situated beneath the Eastern Carpathians in Romania and is characterized by well-confined and persistent intermediate-depth activity (60 km < depth < 220 km). In this study, we have used an updated version of the Trifu & Radulian (1991) catalogue for this area. The initial catalogue consists of 5630 intermediate-depth events with $Mw \geq 1.5$, occurring between 1974 and 2002. The magnitude of completeness of the catalogue slightly increases with depth, being on average around 2.6 (Trifu & Radulian 1991). Therefore, we have selected for analysis earthquakes with $M \geq 2.6$, and decluster the catalogue as explained at the end of this section. The resulting data set has 4254 events (Fig. 4a). A detailed description of the catalogue and its main statistical features can be found in Trifu *et al.* (1990), Trifu & Radulian (1991) and Enescu *et al.* (2003).

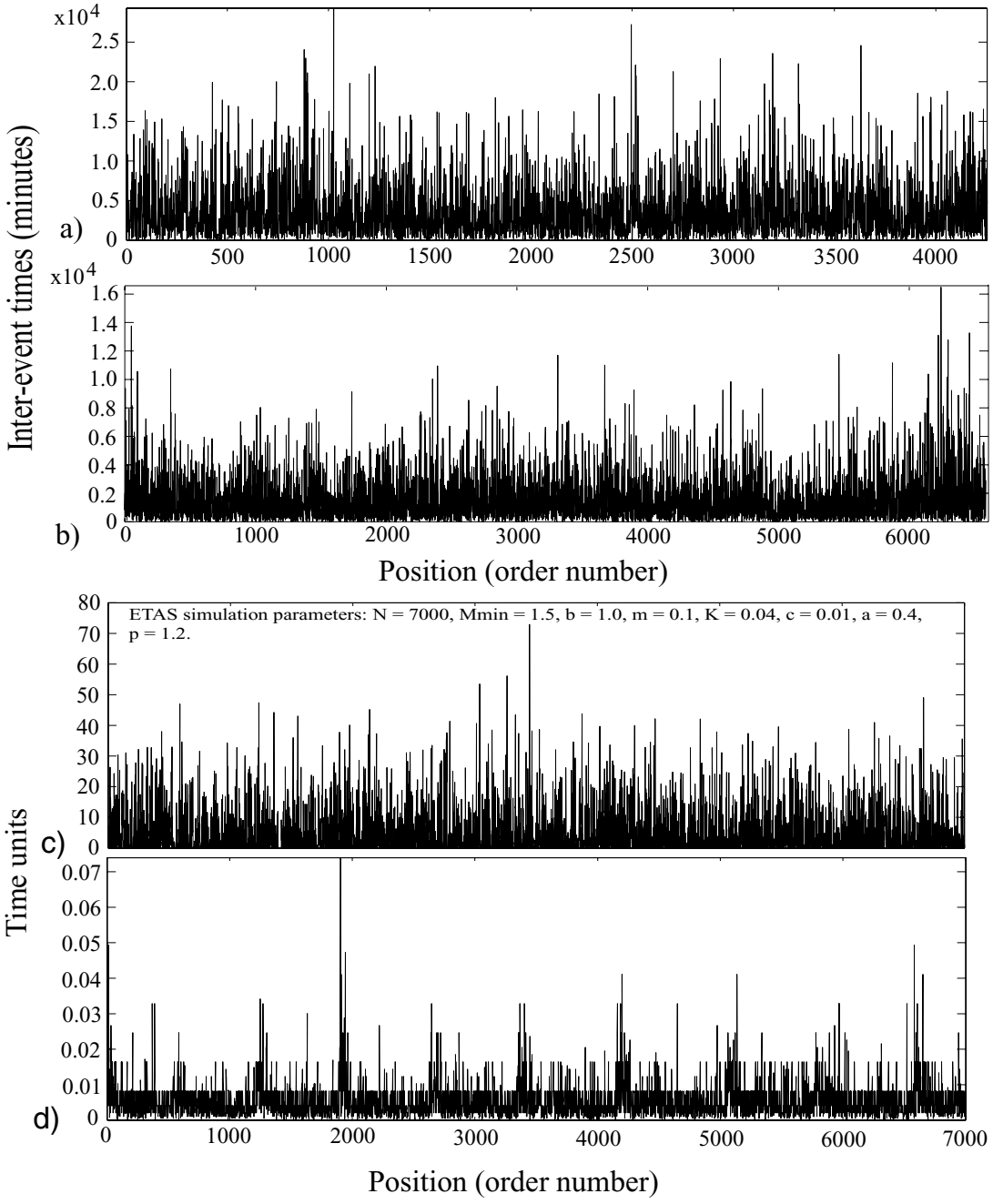

Figure 4. Records of interevent times, that is, earthquake intervals, in the case of: (a) the Vrancea (Romania) earthquakes; (b) the shallow seismicity in the Hyogo region; (c) ETAS model simulation and (d) EBZ_A simulation. For case (d) only 7000 earthquake intervals were represented to show clearly the temporal pattern.

The seismic activity before the 1995 Kobe earthquake

The second case studied is represented by the crustal seismic activity (depth $\leq$30 km), which occurred in the northern Hyogo area, Japan, from 1976 to 1995 January 17, the date of the Kobe earthquake ($Mw = 6.9$), in a broad area surrounding the epicentre of the large event. We have used the earthquake catalogue of the Disaster Prevention Research Institute, Kyoto University, which for the area and period under investigation, is complete in earthquakes of magnitude $M \geq 1.5$ (Enescu & Ito 2001). The good coverage with seismic stations in the region and the phase picking, which was done by a person on the basis of the same criteria throughout the period, produced a homogeneous, high-quality catalogue. The selection of a relatively large area (34–36°N and 134–136°E) for analysis is mainly motivated by the spatial extent of the stress-change-related phenomena which were reported taking place before and after the occurrence of the 1995 Kobe earthquake. More precisely, there is clear evidence of earthquake triggering in this broad region after the occurrence of the large event (Katao & Ando 1996; Hashimoto 1996; Enescu & Ito 2001). Moreover, there are several well-documented reports (after the event) on the premonitory phenomena which have occurred within this large area several years before the 1995 Kobe earthquake: seismicity rate decrease and increase, *b*-value and fractal dimension anomalous changes (e.g. Watanabe 1998; Enescu & Ito 2001; Enescu 2004; Ogata 2004).

The original and the declustered (6583 events, Fig. 4b) data sets were thoroughly tested statistically by Enescu & Ito (2001) and, in his PhD thesis, by Enescu (2004). Therefore, we refer to these studies for further details.

ETAS model simulation

The ETAS model (Ogata 1985, 1988) is a point process model representing the activity of earthquakes of magnitude *Mc* and larger occurring in a certain region during a certain interval of time. We have simulated such a process by using the following parameters: $Mc = 1.5, b = 1.0, \mu = 0.1, K = 0.04$. $c = 0.01, \alpha = 0.4$ and $p = 1.2$ (Fig. 4c). The first parameter represents the magnitude of completeness for the simulated data. The *b*-value is the slope of the frequency-magnitude distribution of earthquakes. The following five parameters represent the characteristics of earthquakes in the simulated time-series. Among them, the last two parameters, α and p, are the most important in describing the temporal pattern of seismicity. Thus, the p-value describes the decay rate of aftershock activity, and the α-value measures the efficiency of an earthquake with a certain magnitude to generate offspring, or aftershocks, in a wide sense. For the physical interpretation of the other parameters and more details, we refer to Ogata (1992). In this study we have chosen a small α-value to simulate a sequence of 7000 events, with 'low productivity' of aftershocks.

Simulation of seismicity by using a 2-D heterogeneous fault embedded in a 3-D elastic half-space

The model we use (Ben-Zion 1996) generates seismicity along a fault segment that is 70 km long and 17.5 km deep. The fault is divided into square cells with dimensions of 550 m. The boundary conditions and model parameters are compatible with the observations along the central San Andreas Fault. Eneva & Ben-Zion (1997) applied several pattern recognition techniques to examine four realizations of the model, with the same creep properties, but different brittle properties. The simulated catalogue of this study is identical to the case (A), described by Eneva & Ben-Zion (1997), and is the result of a fault model containing a Parkfield-type asperity of size 25 km $\times$ 5 km. From now on we will refer to this simulation as EBZ_A (25 880 events in total; Fig. 4d).

We decided to decluster both 'real' earthquake catalogues before analysis (i.e. to eliminate the aftershock sequences from the catalogues) for two main reasons:

(a) We are more interested in searching for LRD in the catalogue and, therefore, the elimination of shorter-range dependent seismicity (i.e. aftershocks) is considered appropriate, since it may influence the results on LRD.

(b) The magnitude of completeness might be subevaluated immediately after the occurrence of some larger events, during the periods and in the regions under study. However, in the case of the intermediate-depth Vrancea earthquakes, the number of aftershocks is small even after major earthquakes, such as those that occurred in 1977 ($Mw = 7.4$), 1986 ($Mw = 7.1$) and 1990 ($Mw = 6.9$). For the crustal, shallow events in the Hyogo area, there are no major earthquakes during the period of investigation.

In the case of the shallow earthquakes in the northern Kinki region, the declustering was done by using Reasenberg's (1985) algorithm. Details on the results of the aftershock removal procedure and the robustness of the declustering algorithm applied to this sequence of events, can be found in Enescu & Ito (2001) and Enescu (2004). For the Vrancea (Romania) earthquakes a simplified declustering procedure was adopted, taking advantage of the scarcity of aftershocks for these intermediate-depth events (Enescu *et al.* 2003). The declustered catalogue was obtained by eliminating the aftershock sequences following the three major earthquakes that occurred in 1977, 1986 and 1990. The abnormal aftershock activity occurs in time windows of several months, but is especially concentrated in the first hours and days following the occurrence of a major event. As reported by Enescu *et al.* (2003), the scaling range of the aftershocks and the declustered seismicity is different in Vrancea region and, therefore, one can characterize unambiguously their fractal properties.

5 RESULTS AND DISCUSSION

Fig. 4 shows the series of interevent times between consecutive earthquakes for all four cases studied. The graphs look rather similar, with no clear distinctive characteristics. Only the EBZ_A simulation (Fig. 4d) shows some kind of regular and quasi-periodic behaviour.

Fig. 5(a) shows the CWT representation in the case of the Vrancea region earthquake intervals. A zoomed view is displayed in order to observe better the clear self-similar (*fractal*) pattern. From an intuitive point of view, the wavelet transform consists of calculating a 'resemblance index' between the signal and the wavelet, in this case the second derivative of the *Gaussian*. If a signal is similar to itself at different scales, then the 'resemblance index' or wavelet coefficients also will be similar at different scales. In the coefficients plot (Fig. 5a), which shows scale on the vertical axes, this self-similarity generates a characteristic pattern. We believe that this is a very good demonstration of how well the wavelet transform can reveal the fractal pattern of the seismic activity at different times and scales. Fig. 5(b) displays the maxima lines of the CWT (i.e. the WTMM tree) in the case of the Vrancea time-series. One can notice the branching structure of the WTMM skeleton, in the (*position, scale*) coordinates, which enlightens the hierarchical structure of time-series singularities.

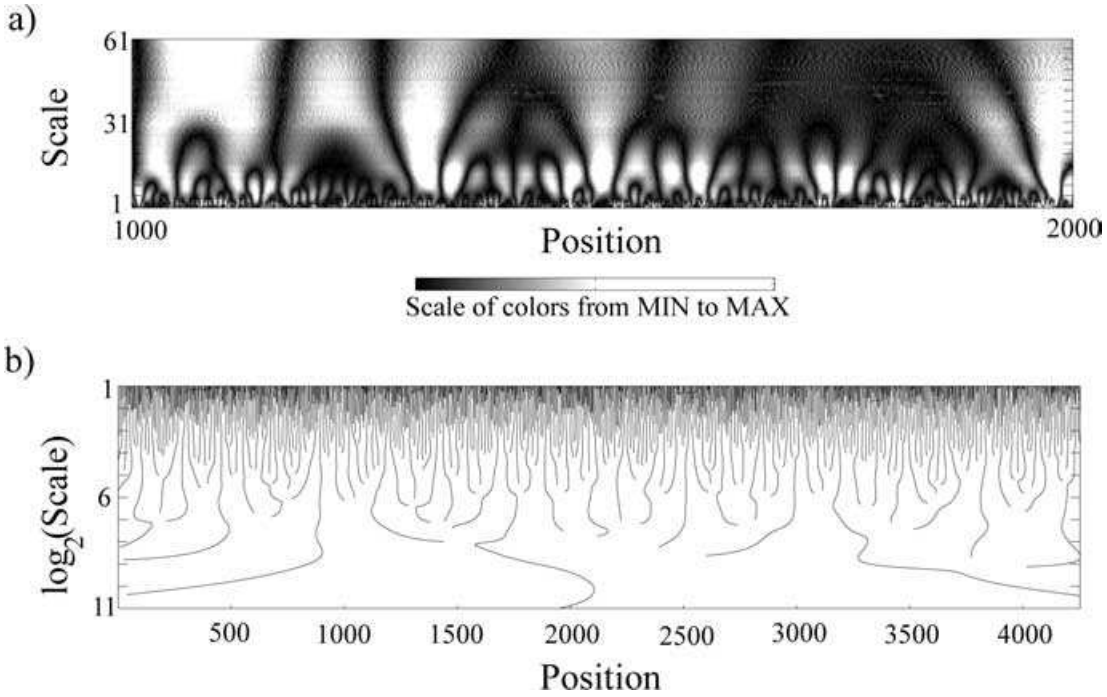

Figure 5. (a) CWT coefficients plot in the case of the Vrancea (Romania) time-series, zoomed view. Scale and position are on the vertical and horizontal axes, respectively. The coefficients, taking values between *MIN* and *MAX*, are plotted by using 64 levels of grey. The plot was obtained by using the 'Wavelet toolbox' of Matlab software. (b) WTMM skeleton plot. The vertical axis is logarithmic, with small scales at the top.

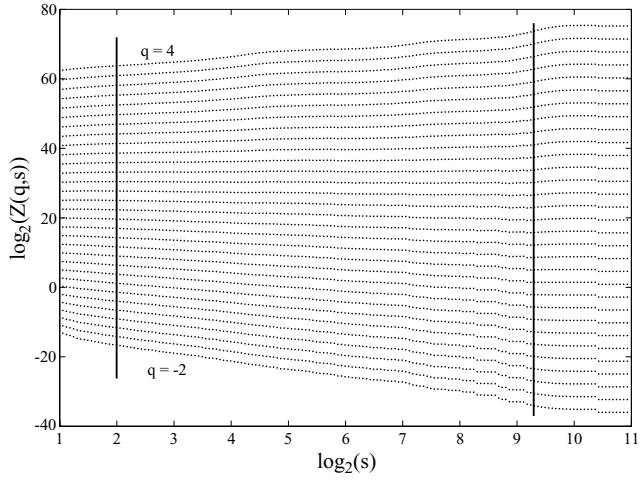

Figure 6. Double logarithmic plot of the partition functions, for q between 4 to -2 (up to down, constant increment), in the case of the Vrancea time-series. The vertical lines indicate the limits of the scaling region. Outside this area there are 'boundary effects' due to the limited length of the time-series.

Fig. 6 represents in a logarithmic plot the partition functions $Z(q, s)$ versus scale (s), obtained from the WTMM skeleton representation (Fig. 5b). One can notice the existence of a well-defined, relatively broad scaling region, as it is indicated in the figure. This scaling domain corresponds approximately to time periods from days to several years.

Fig. 7 shows the $D(h)$ plot in the case of the Vrancea (Romania) integrated interevent times. The spectrum is narrow (i.e. the Hurst exponent (h) takes values in a very limited range). The τ spectrum, represented in the inset of the figure, can be well fitted by a straight line. These observations suggest that our time-series is the result of a monofractal (or near-monofractal) process. One can also notice that the 'central' h-value of the spectrum is close to 0.5, which is an indication of the nearly random behaviour of the time-series. Enescu *et al.* (2005) obtained a similar result, by using a 'monofractal' approach, the DFA technique. Therefore, we cannot reject the null hypothesis that the defining temporal characteristics of the analysed data set ($M \geq 2.6$) are monofractality and randomness.

Before presenting the results concerning our second earthquake sequence, we would like to illustrate, using a simple example, the effect of artificial trends on the results of fractal analysis, when a non-detrending technique is used. Fig. 8(a) shows the cumulative number of events versus time for an 'artificial' sequence of events obtained from the seismic catalogue in Vrancea region by selecting earthquakes with $M \geq 2.6$ for time period $T1$ (1976–1985) and $M \geq 3.2$ for $T2$ (1985–2002). In this way, we can simulate an (artificial) change of seismicity rate, which could be, for example, the result of a different detection capability of the seismic network during the two time periods. In real earthquake catalogues seismicity rate changes could be more complex, however, we consider that the simple 'pattern' considered here has the characteristics and appearance (Fig. 8a) of a realistic simulation.

To study this sequence we apply the Hurst analysis (known also as rescaled range or R/S analysis), a standard technique used to detect correlations of noisy time-series (Hurst 1951). In the context of earthquakes, the method has been applied by Lomnitz (1994) and Goltz (1997), among others. A good introduction can be found in Feder (1988) and Turcotte (1997). For a time-series $u(i)$ ($i = 1, 2, 3 \ldots, N\text{max}$), it is divided into boxes of equal size n. In each box, the cumulative departure X_i of the series from the mean is calculated. The range, R, is defined as the difference, max (X_i) − min (X_i), in each box. One can compute then R/S, where S is the standard deviation and obtain the average of the rescaled range, $\langle R/S \rangle$, in all boxes of equal size n. Repeat the above computation

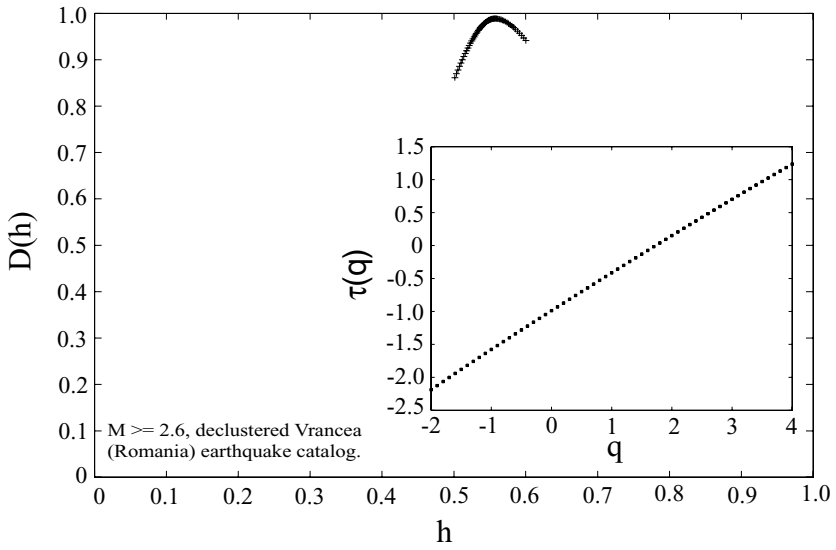

Figure 7. $D(h)$ spectrum of the integrated interevent times, in the case of the Vrancea (Romania) integrated earthquake intervals. The spectrum is nearly monofractal, centred on 0.56. This value, slightly larger than 0.5, is an indication of quasi-randomness. The inset shows the $\tau(q)$ spectrum, which is very close to a straight line (an indication of monofractality).

over different box sizes, n, to provide a relationship between $\langle R/S \rangle$ and n. According to Hurst's experimental study (Hurst 1951), a power-law relation between $\langle R/S \rangle$ and n indicates the presence of scaling: $\langle R/S \rangle \sim n^H$, where H is the Hurst exponent. Since the Vrancea region sequence of earthquakes is monofractal, one has $h = H$ (Section 2).

If our sequence of events is analysed separately during the periods $T1$ and $T2$, by using R/S analysis, we obtained $H = 0.56$ and $H = 0.57$, respectively. This is in rather good agreement with our wavelet-based results, which showed quasi-randomness in Vrancea's case. However, if we analyse together all data, the resulting $\langle R/S \rangle$ graph (Fig. 8b) shows two different scaling regions. At small scales we obtain $H = 0.56$, while at large scales the Hurst exponent is 0.9! The large value of H would suggest non-random, highly correlated behaviour at large scales. Obviously, the large Hurst exponent does not reflect correlation or clustering of the catalogue, but is just a spurious effect of the seismicity rate change, or, in other words, of the non-stationarity of the data. Of course, in this simple, illustrative example, we can easily detect the rate change and choose to investigate the two time periods, $T1$ and $T2$, separately. However, by doing so, the results will be less accurate due to the shorter length of each time-series. Moreover, in real catalogues there might be several such rate changes and, thus, one could not afford anymore partitioning the data.

By applying the WTMM approach to the same data set, we have obtained unbiased results, similar with those in Fig. 7: a narrow $D(h)$ singularity spectrum, centred on 0.55.

Simple trends, caused by artificial (man-made) or natural phenomena can be seen frequently in real earthquake catalogues. If one is interested in the real fractal properties of earthquakes and their genuine LRD, the wavelets provide the necessary tool to look beyond these non-stationarities. Moreover, there are other known shortcomings of the R/S analysis, as for example the difficulty to discriminate between long- and short-range correlations of a time-series.

Fig. 9 shows the partition functions $Z(q, s)$ computed from the WTMM skeleton of the second time-series considered here for analysis: the interevent times of the 'Kobe sequence'. One can easily notice that there are two distinct, well-defined, scaling domains, at smaller scales and larger ones respectively, as indicated in the figure. Further evidence for the existence of these two scaling regions is presented in Fig. 10, which displays the amplitude of the *Wavelet Transform* along *Ridges* (i.e. maxima lines). As eq. (4) also suggests, the slopes of these maxima lines correspond to the local Hölder exponents (or local singularities) of a time-series. However, for most 'real' signals, these 'local' slopes are intrinsically unstable (mainly because the singularities are not isolated), thus making very difficult the estimation of these local exponents. In contrast, the partition function approach provides global estimates of scaling, which are statistically more robust. However, by closely examining Fig. 10, one can notice that again there is a rather clear crossover between small and large scales.

By computing the corresponding $D(h)$ spectrum for each of the two scaling domains, at small scales ($2^1 \sim 2^4$) we observed multifractal behaviour, while at larger scales ($2^4 \sim 2^9$) the series is monofractal, with an exponent of about 0.8. The first scaling domain extends roughly from hours to days, while the second one corresponds to periods of time up to 2–3 yr. As is known, $h > 0.5$ could indicate the presence of correlations (or long-range correlations), but there is also another important factor that can produce $h > 0.5$. It relates to the probability distribution of the time-series (in our case the probability distribution of the interevent times). Thus, for series with a power-law-like probability distribution (or other distributions characterized by heavy tails), one observes $h > 0.5$. A method to discriminate between LRD and the results of the probability distribution effects is to analyse the shuffled version of the signal. A shuffling technique was also used by Huc & Main (2003) to develop a null hypothesis for examining earthquake triggering on a global scale. By shuffling the series, the correlation is lost but the power-law-like distribution, if present, remains unchanged. In other words, the shuffled series would have $h = 0.5$ in the first case (only LRD) and $h > 0.5$ in the second one (only power-law-like distribution). We shuffled our series and obtain $h = 0.5$, which excludes the possibility of an h larger than 0.5 caused by the probability distribution.

There is still one more factor that could 'induce' LRD-like characteristics: the presence of trends within the data. As already

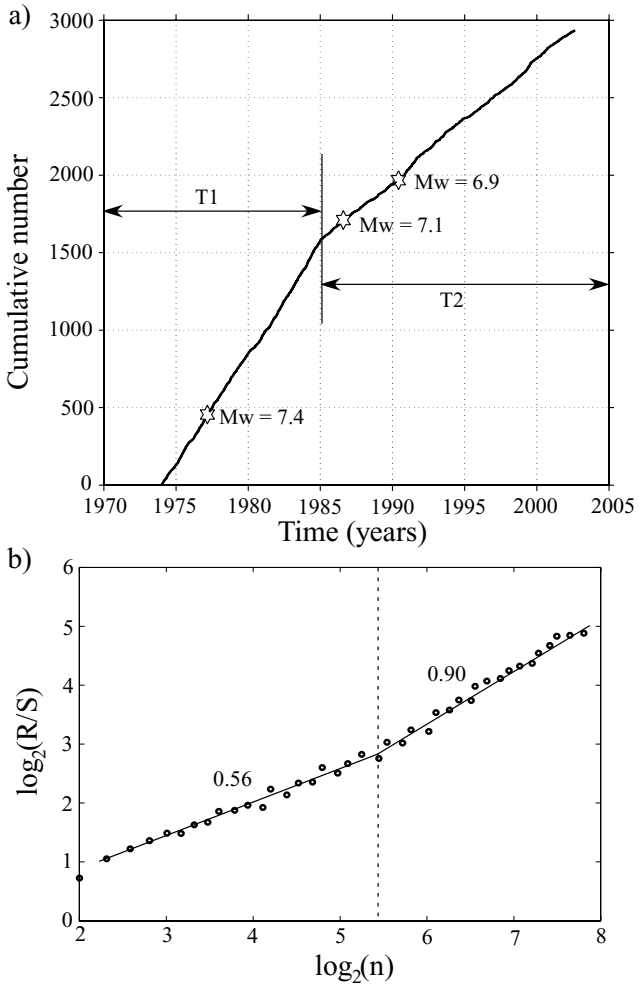

Figure 8. (a) Cumulative number of events for the 'artificial' Vrancea earthquake time-series (see text for details). The earthquakes occurred during time periods $T1$ and T2 have threshold magnitudes of 2.6 and 3.2, respectively. (b) Rescaled range (R/S) analysis of the data in Fig. 8(a). One can clearly notice the crossover of scaling (marked by a vertical dotted line). The numbers indicate the slopes of the graph and hence the Hurst exponents in the two regions.

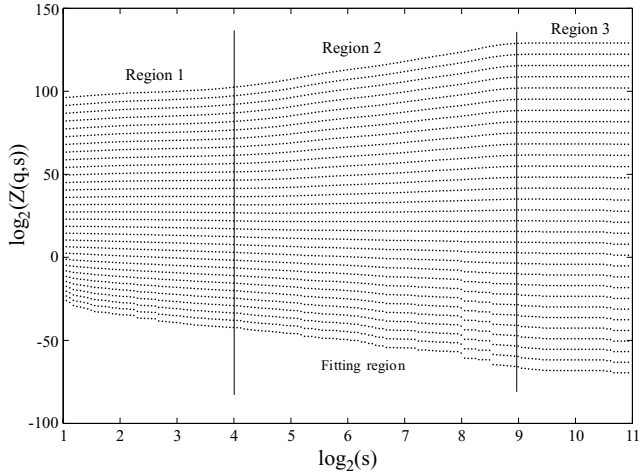

Figure 9. Partition functions for q between 7 to -4 (from up to down, constant increment), for the case of the 'Kobe time-series'. One can notice a clear crossover of scaling between Region 1 and Region 2. There is no reliable scaling in Region 3, due to the limited length of the data set.

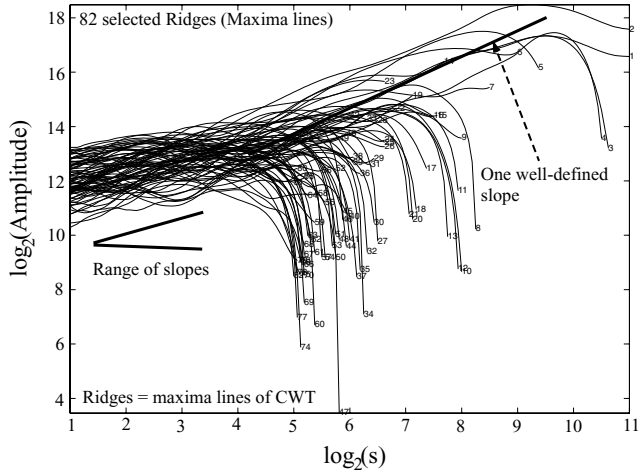

Figure 10. Logarithmic plot of the amplitude of CWT along ridges (maxima lines of the *continuous wavelet transform*) in the case of the 'Kobe sequence'. At large scales there is only one well-defined, predominant slope of the lines, while at smaller scales there is a range of slopes. Because of the large number of WTMM lines, only a representative set was considered in this plot.

mentioned, the wavelet approach eliminates the effect of polynomial trends, if an appropriate mother wavelet is used to compute the CWT. However, there are situations when other types of trends are present in the time-series, like for example power-law or oscillatory trends. As shown by Kantelhardt *et al.* (2001) and Hu *et al.* (2001), both kinds of non-stationarities, superposed on LRD data, could produce crossovers of the scaling region. By carefully analysing our sequence, we identified some oscillatory behaviour and also periods of 'accelerating seismicity' or quiescence. As shown by Enescu & Ito (2001) and Enescu (2004) anomalous earthquake frequency changes occurred several years before the 1995 Kobe earthquake. The increase and decrease of earthquake frequency could have been associated with power-law (or higher order polynomial?) trends of the earthquake intervals. Therefore, it is possible that such rather complex non-stationary patterns are responsible for the large value of h and thus for the LRD signature obtained in this study. We would like to note, however, that while a clear distinction should be made between simple, trivial trends and genuine LRD, such a separation is probably less definite in the case of trends having complex, low-frequency characteristics. On the other hand, more important to emphasize in our case is the existence of two distinct scaling domains, both of them associated with fluctuations that are *intrinsic* to the data. More research has to be done, however, to identify 'the nature' of these fluctuations and their physical background.

The computation of the $D(h)$ spectrum at small scales (2^1 to 2^4; see Fig. 9) showed multifractality, which probably corresponds to inhomogeneous local scaling behaviour of the time-series. The result may also reflect the incomplete detection and removal of aftershocks. However, these findings are less reliable due to the limited length of the data set and a rather short scaling domain.

Our third case is concerned with the analysis of a simulated earthquake sequence, obtained by using the ETAS model. Fig. 11 shows the $D(h)$ spectrum computed by using a scaling region of the partition functions Z between 2^3 and 2^{10}. The plot shows a monofractal spectrum, with a Hurst exponent, h, close to 0.5. It is an expected

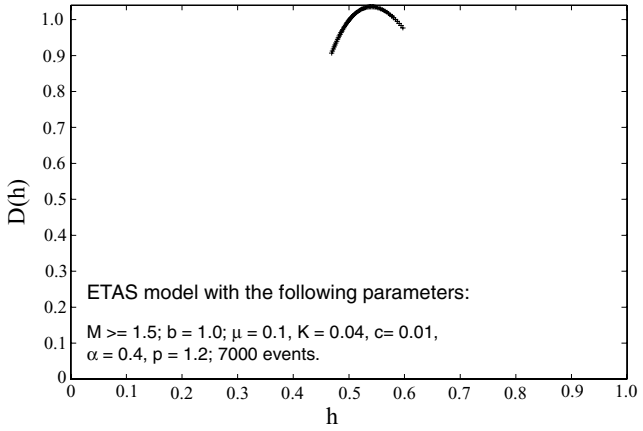

Figure 11. Multifractal spectrum in the case of ETAS model simulation. By analysing the spectrum one can assume a nearly monofractal, non-correlated process. A scaling range between 2^2 and 2^9 was used to compute the $D(h)$ spectrum.

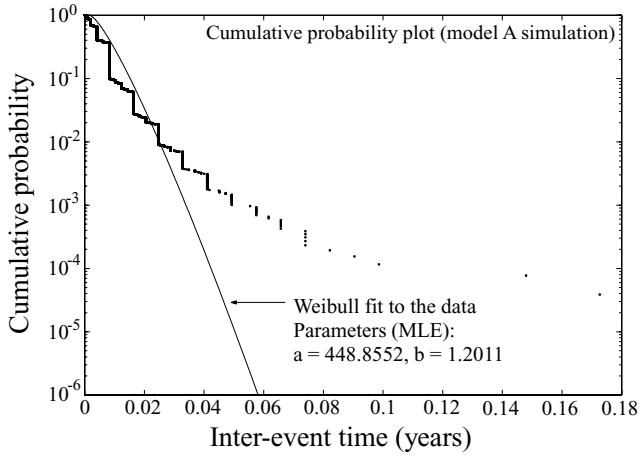

Figure 12. Cumulative probability plot of interevent times distribution (IDT) for 'model' A simulation. A Weibull probability distribution, $w(IDT) = ab(IDT)^{b-1} \exp(-a(IDT)^b)$, is fitted to the data. The maximum likelihood estimates of parameters a and b are shown in the graph. For a Poisson process, it is expected that $b = 1$ and the graph would become a straight line. If earthquakes tend to occur in clusters, $0 < b < 1$. If they occur intermittently or nearly periodically, $b > 1$.

finding for a sequence that has low offspring productivity and thus behaves quasi-randomly in the range of scales mentioned above. The result demonstrates that the small number of aftershocks, which occurred for very short periods of time, could not influence significantly the spectrum's characteristics at larger scales.

Our final analysis is concerned with another earthquake simulation, EBZ_A (see chapter 3). We are primarily interested here to see if oscillatory behaviour of the time-series could induce a crossover of scaling and apparent long-range correlation. Fig. 12 shows the result of basic statistical testing of data. We represent the cumulative probability distribution of the interevent times in a half-logarithmic plot. A random occurrence of earthquakes corresponds to an exponential distribution of the interevent times and, thus, in such a case, one would expect a straight line of the plot. The evident departure from linearity is a clear proof that the simulated earthquakes do not occur randomly. The step-like shape of the plot suggests that some

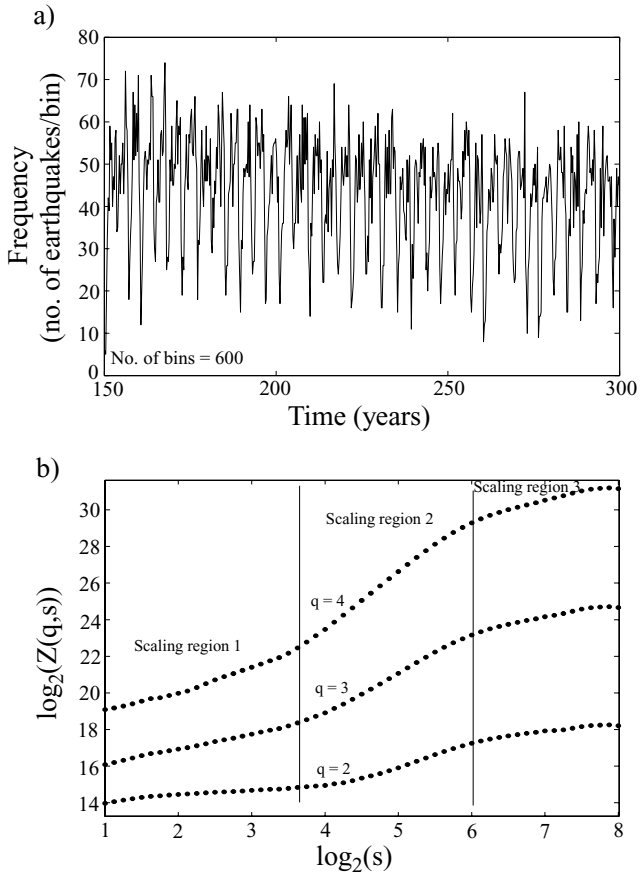

Figure 13. (a) Frequency of earthquakes versus time plot, in the case of EBZ_A simulation. Oscillatory behaviour is observed. (b) Partition functions, Z, for $q = 2$, 3, 4, in the case of EBZ_A simulation. Several distinct scaling domains are observed. The vertical lines indicate the approximate borders of these regions.

recurrence intervals are strongly preferred, or in other words that our synthetic data has several quasi-periodicities.

Fig. 13(a) presents the frequency of earthquakes versus time (the total time span of the earthquake sequence is 150 yr). The graph confirms the periodic behaviour found before. We have also analysed the variation of CWT coefficients with time and found the same oscillatory behaviour. Fig. 13(b) displays the partition functions in the case of the EBZ_A simulation, only for $q = 2$, 3 and 4. As in the case of the 'Kobe earthquake time-series', one can see a segmented plot, which indicates different characteristics across scales. It is beyond the scope of this study to analyse in detail the influence of oscillatory trends on the multifractal characteristics of the analysed signal, as they are revealed by wavelet analysis. Some preliminary results, however, indicate that such a relation could be 'quantified' and employed as a useful tool to analyse the behaviour of complex signals.

Finally we would like to note that the results reported so far on real seismicity are stable when we 'sample' the catalogues in different ways: chose a different threshold magnitude, analyse the data for different spatial and temporal windows.

6 CONCLUSIONS

The present paper presents an in-depth analysis of the multifractal and correlation properties of real and simulated time-series of

earthquakes, using a new, wavelet-based approach. Our study reveals the clear fractal pattern of the analysed series of interevent times and their different scaling characteristics.

In the case of the intermediate-depth seismic activity in Vrancea, Romania, we found random and monofractal behaviour that occurs for a rather broad range of scales. The crustal seismic activity in the Hyogo area, Japan, has different characteristics, the most notable ones being the crossover in scaling and the long-range correlation signature observed at larger scales. It is not certain, however, what is the 'nature' of this LRD-like behaviour. We believe that the complex non-stationarities of the data (trends) are responsible for this result. There is some evidence in support of our assumption, coming from theoretical studies of LRD with superposed oscillatory or power-law trends. The precise mechanism of the observed LRD needs to be analysed further with the wavelet transform. We believe it is essential to studying this phenomenon since it is ultimately related to the predictability of the earthquake time-series.

The investigation of two simulated earthquake sequences helped to understand the fractal and correlation properties of the real data. Thus, the analysis of the ETAS model sequence, with a 'low productivity' of aftershocks, showed that the clustering that occurs 'locally' does not have any influence on the results at larger scales. The investigation of the time-series of earthquakes simulated by using a cellular fault embedded in a 3-D elastic medium revealed the quasi-cyclic behaviour of the earthquake occurrence. We have shown that there are several crossovers of scaling, which are probably associated with the oscillatory trends of the simulated sequence of earthquakes.

As one could notice, the present study does not indicate explicit confidence intervals for the h-value estimates. We briefly discuss here this issue. In the case of the *Multinomial Cantor Measure* (Section 3), we have generated a large number of series (100) having the same length (4096) and determined for each of them the $D(h)$ singularity spectrum. For $q = 10$, the computed h-values form a distribution centred on the theoretical h-value (0.28), with a standard deviation of ± 0.05. The standard deviation of h for other q-values is smaller. Because the analysed earthquake time-series have lengths larger than 4096, one would expect even smaller standard deviations. In reality, the effective uncertainty in the case of earthquake data is probably larger since we do not have the perfect multifractal behaviour of the *Multinomial Cantor Measure.* Surrogate data, obtained for example by randomly shuffling the original series, should be used to test for the significance of the results.

The fractal characteristics of our time-series were mainly addressed in this study by computing 'global estimates of scaling'. However, by using a recently developed technique (Struzik 1999), one can evaluate the Hölder exponent at an arbitrary location and scale. Such an approach has led to interesting findings in different fields, such as medicine (Ivanov *et al.* 1999) and the economy (Struzik 2001). In our next studies we are planning to follow such a 'local' approach to study the complexity of earthquake time-series. Moreover, by using a 2-D wavelet transform, we would like to extend our research from time-series to spatial patterns of seismicity.

ACKNOWLEDGMENTS

We would like to thank Prof. Y. Ogata, Prof. Y. Ben-Zion and Dr M. Anghel for useful discussions and for providing simulation software programs and data. We acknowledge the useful comments and suggestions of Professors J. Mori, Y. Umeda, I. Kawasaki and I. Nakanishi. We are grateful to Dr R. Clark, Prof. C. Ebinger, and an anonymous reviewer for their critical comments, which improved the quality of this study. BE is grateful to the Japanese Ministry of Education for providing him a scholarship to study at Kyoto University, Japan.

REFERENCES

Arneodo, A., Bacry, E. & Muzy, J.F., 1991. Wavelets and multifractal formalism for singular signals: application to turbulence data, *Phys. Rev. Lett.,* **67,** 3515–3518.

Arneodo, A., Bacry, E. & Muzy, J.F., 1995. The thermodynamics of fractals revisited with wavelets, *Physica A,* **213,** 232–275.

Badii, R. & Broggi, G., 1988. Measurement of the dimension spectrum $f(\alpha)$: fixed-mass approach, *Physics Letters A,* **131**(6), 339–343.

Ben-Zion, Y., 1996. Stress, slip and earthquakes in models of complex single-fault systems incorporating brittle and creep deformations, *J. geophys. Res.,* **101,** 5677–5706.

Ben-Zion, Y. & Rice, J.R., 1993. Earthquake failure sequences along a cellular fault zone in a three-dimensional elastic solid containing asperity and non-asperity regions, *J. geophys. Res.,* **98**(B8), 14 109–14 131.

Buckheit, J.B. & Donoho, D.L., 1995. Wavelab and reproducible research, in *Wavelets and Statistics*, pp. 55–81, eds Antoniadis, A. & Oppenheim, G., Springer Verlag, New York.

Enescu, B., 2004. Temporal and spatial variation patterns of seismicity in relation to the crustal structure and earthquake physics, from the analyses of several earthquake sequences in Japan and Romania, *PhD thesis,* Kyoto University, Kyoto, Japan.

Enescu, B. & Ito, K., 2001. Some premonitory phenomena of the 1995 Hyogo-ken Nanbu earthquake: seismicity, b-value and fractal dimension, *Tectonophysics,* **338**(3–4), 297–314.

Enescu, B., Ito, K., Radulian, M., Popescu, E. & Bazacliu, O., 2005. Multifractal and chaotic analysis of Vrancea (Romania) intermediate-depth earthquakes—investigation of the temporal distribution of events, *Pure appl. Geophys.,* **162,** 249–271.

Eneva, M. & Ben-Zion, Y., 1997. Application of pattern recognition techniques to earthquake catalogs generated by model of segmented fault systems in three-dimensional elastic solids, *J. geophys. Res.,* **102**(B11), 24 513–24 528.

Feder, J., 1988. *Fractals*, Plenum Press, New York.

Geilikman, M.B., Golubeva, T.V. & Pisarenko, V.F., 1990. Multifractal patterns of seismicity, *Earth and Planetary Science Letters,* **99,** 127–132.

Goltz, C., 1997. *Fractal and chaotic properties of earthquakes*, Springer Verlag, Berlin.

Grassberger, P., Badii, R. & Politi, A., 1988. Scaling laws for invariant measures on hyperbolic and nonhyperbolic attractors., *J. Stat. Phys.,* **51,** 135–178.

Hashimoto, M., 1996. Static stress changes associated with the Kobe earthquake: calculation of changes in Coulomb failure function and comparison with seismicity change, *J. Seismol. Soc. Jpn.,* **48,** 521–530 (in Japanese with English abstract).

Hirabayashi, T., Ito, K. & Yoshii, T., 1992. Multifractal analysis of earthquakes, *Pure appl. Geophys.,* **138**(4), 591–610.

Hu, K., Ivanov, P.Ch., Chen, Z., Carpena, P. & Stanley, H.E., 2001. Effect of trends on detrended fluctuation analysis, *Physical Review E,* **64,** 011114-1: 011114-19.

Huc, M. & Main, I.G., 2003. Anomalous stress diffusion in earthquake triggering: correlation length, time dependence, and directionality, *J. geophys. Res.,* **108**(B7), 2324, doi:10.1029/2001JB001654.

Hurst, H.E., 1951. Long-term storage capacity of reservoirs, *Trans. Am. Soc. Civil Eng.,* **116,** 770–799.

Ivanov, P.Ch., Amaral, L.A.N., Goldberger, A.L., Havlin, S., Rosenblum, M.G., Struzik, Z.R. & Stanley, H.E., 1999. Multifractality in human heartbeat dynamics, *Nature,* **399,** 461–465.

Kagan, Y.Y. & Jackson, D.D., 1991. Long-term earthquake clustering, *Geophys. J. Int.,* **104,** 117–133.

Kantelhardt, J.W., Koscienly-Bunde, E., Rego, H.H.A., Havlin, S. & Bunde, A., 2001. Detecting long-range correlations with detrended fluctuation analysis, *Physica A,* **295,** 441–454.

Katao, H. & Ando, M., 1996. Crustal movement before and after the Hyogo-ken Nanbu earthquake, *Kagaku,* **66,** 78–85 (in Japanese).

Lomnitz, C., 1994. *Fundamentals of Earthquake Prediction*, John Wiley & Sons, New York.

Mallat, S., 1999. *A wavelet tour of signal processing*, Academic Press, San Diego.

Mallat, S. & Hwang, W.L., 1992. Singularity detection and processing with wavelets, *IEEE Trans. on Information Theory,* **38,** 2.

Mulargia, F. & Geller, R.J., 2003. *Earthquake Science and Seismic Risk Reduction*, Kluwer Academic Publishers, Dordrecht.

Muzy, J.F., Bacry, E. & Arneodo, A., 1994. The multifractal formalism revisited with wavelets, *Int. J. Bifurc. Chaos,* **4,** 245–302.

Ogata, Y., 1985. Statistical models for earthquake occurrences and residual analysis for point processes, *Res. Memo.* (Technical Report) 288, Inst. Statist. Math., Tokyo.

Ogata, Y., 1988. Statistical models for earthquake occurrences and residual analysis for point processes, *J. Amer. Statist. Assoc.,* **83,** 9–27.

Ogata, Y., 1992. Detection of precursory relative quiescence before great earthquakes through a statistical model, *J. geophys. Res.,* **97**(B13), 19 845–19 871.

Ogata, Y., 2004, Space-time model for regional seismicity and detection of crustal stress changes, *J. geophys. Res.,* **109,** B03308, doi: 10.1029/2003JB002621.

Ouillon, G. & Sornette, D., 1996. Unbiased multifractal analysis; application to fault patterns, *Geophys. Res. Lett.,* **23,** 3409–3412.

Peitgen, H.O., Jurgens, H. & Saupe, D., 1992. *Chaos and fractals*, New frontiers of science, Springer Verlag, New York.

Reasenberg, P., 1985. Second-order moment of central California seismicity, 1969-1982, *J. geophys. Res.,* **90**(B7), 5479–5495.

Smalley, R.F., Jr, Chatelain, J.-L., Turcotte, D.L. & Prevot, R., 1987. A fractal approach to the clustering of earthquakes: applications to seismicity of the New Hebrides, *Bull. seism. Soc. Am.,* **77,** 1368–1381.

Struzik, Z.R., 1999. Local effective Hölder exponent: estimation on the wavelet transform maxima tree, in *Fractals: Theory and Applications in Engineering*, 93–112, Dekking, M., Vehel, J.L., Lutton, E. & Tricot, C., Springer Verlag, London.

Struzik, Z.R., 2001. Wavelet methods in (financial) time series processing, *Physica A,* **296**(1–2), 307–319.

Torrence, C. & Compo, G.P., 1998. A practical guide to wavelet analysis, *Bulletin of the American Meteorological Society,* **79**(1), 61–78.

Trifu, C.-I. & Radulian, M., 1991. Frequency-magnitude distribution of earthquakes in Vrancea: relevance for a discrete model, *J. geophys. Res.,* **96**(B3), 4301–4311.

Trifu, C.-I., Radulian, M. & Popescu, E., 1990. Characteristics of intermediate depth microseismicity in Vrancea region, *Rev. Geofis.,* **46,** 75–82.

Turcotte, D.L., 1989. Fractals in geology and geophysics, *Pure appl. Geophys.,* **131,** 171–196.

Turcotte, D.L., 1997. *Fractals and Chaos in Geology and Geophysics*, 2nd edn, Cambridge University Press, Cambridge.

Watanabe, H., 1998. The 1995 Hyogo-ken-Nanbu earthquake and the accompanying seismic activity—behaviour of the background seismicity, *Ann. Disas. Prev. Res. Inst., Kyoto Univ.,* **41A,** 25–42 (in Japanese with English abstract).